

# Symmetric “Double Spiro” Wide Energy Gap Hosts for Blue Phosphorescent OLED Devices

Jie Ma, Muazzam Idris, Tian Y. Li, Daniel S. M. Ravinson, Tyler Fleetham, Jongchan Kim, Peter I. Djurovich, Stephen R. Forrest, and Mark E. Thompson\*

Wide energy gap materials dispiro[fluorene-9,9'-anthracene-10',9''-fluorene] (SAS) and dispiro[xanthene-9,9'-anthracene-10',9''-xanthene] (XAX) containing double spiro-carbons, are introduced as hosts for blue phosphorescent organic light-emitting diodes (PHOLEDs). Both SAS and XAX are free of heteroatomic exocyclic bonds, which are implicated in limiting the stability of blue PHOLEDs. The materials are synthesized in gram-scale quantities through short and efficient paths. They have large energy gaps ( $\geq 5.0$  eV) between the highest occupied molecular orbital (HOMO) and lowest unoccupied molecular orbital (LUMO) and correspondingly have high triplet energies in solid state ( $E_T \approx 3.0$  eV). Analysis of devices using SAS and XAX as host materials with the blue phosphorescent dopant *fac*-tris(N,N-di-p-tolyl-pyridinoimidazol-2-yl)iridium(III) (Ir(tpz)<sub>3</sub>), shows that charges are transported and trapped by the dopant, which subsequently forms excitons directly on the phosphor. As a result, luminescence quenching pathways are suppressed which leads to blue phosphorescent devices with high ( $\approx 18\%$ ) external quantum efficiency. Thus, SAS and XAX serve as promising host materials, with high triplet energies suitable for blue PHOLEDs.

## 1. Introduction

Phosphorescent organic light-emitting diodes (PHOLEDs) have gained increasing acceptance in flat-panel, flexible displays, and solid-state lighting applications upon the realization of 100% internal quantum efficiency and versatile color tunability.<sup>[1–3]</sup> Even though red and green phosphors have made their way into mass production for displays, short operational lifetimes for blue PHOLEDs have hindered their commercialization.<sup>[4–6]</sup> Among the multiple layers used to construct a PHOLED, the emissive layer, consisting of an emissive dopant and host matrix, plays the most crucial role in determining device performance.<sup>[7–10]</sup> While attention has been paid to the development of stable blue phosphorescent emitters, there is a dearth of stable materials necessary to host blue phosphors.<sup>[11–15]</sup> The challenge to create such hosts is the stringent prerequisites required for these materials, which include: i) a triplet energy ( $E_T$ ) high enough to confine excitons onto the dopant by preventing energy transfer back to the host ( $E_T > 2.8$  eV),<sup>[16–18]</sup> ii) a large energy gap between the highest occupied molecular orbital (HOMO)–lowest unoccupied molecular orbital (LUMO) to promote charge recombination on the dopant,<sup>[19]</sup> iii) strong chemical bonds that are not easily ruptured by the energy of excitons or polarons formed in blue PHOLEDs,<sup>[20,21]</sup> and iv) thermal and morphological stability during device operation.<sup>[22,23]</sup> To the best of our knowledge, no reported host materials satisfy all four criteria for blue PHOLEDs.

Common molecular building blocks for hosts with triplet energies greater than 2.8 eV are shown in **Figure 1**.<sup>[24]</sup> Among these fragments, carbazoles have been widely employed as the core electron-donating moiety in hosts for blue PHOLEDs.<sup>[25]</sup> The carbazole unit is often substituted with electron-accepting groups such as triazine,<sup>[26–29]</sup> pyridine,<sup>[30]</sup> triazole,<sup>[31,32]</sup> phosphine oxide,<sup>[33–38]</sup> and sulfone<sup>[39]</sup> to balance hole and electron transport in the emissive layer. However, intramolecular charge transfer between the electron donor and acceptor units can lower the triplet energy level, despite being separated by poorly conjugating spacers such as arylsilane, phenylene, and fluorene in the molecular backbones.

Both a high triplet energy and a wide HOMO–LUMO gap in the host play crucial roles in forcing charge recombination to


J. Ma, M. E. Thompson  
Department of Materials Science and Engineering  
University of Southern California  
Los Angeles, CA 90089, USA  
E-mail: met@usc.edu

M. Idris, T. Y. Li, D. S. M. Ravinson, T. Fleetham, P. I. Djurovich,  
M. E. Thompson  
Department of Chemistry  
University of Southern California  
Los Angeles, CA 90089, USA

J. Kim, S. R. Forrest  
Department of Electrical Engineering  
University of Michigan  
Ann Arbor, MI 48109, USA

S. R. Forrest  
Department of Physics  
University of Michigan  
Ann Arbor, MI 48109, USA

S. R. Forrest  
Department of Materials Science and Engineering  
University of Michigan  
Ann Arbor, MI 48109, USA

 The ORCID identification number(s) for the author(s) of this article can be found under <https://doi.org/10.1002/adom.202101530>.

DOI: 10.1002/adom.202101530

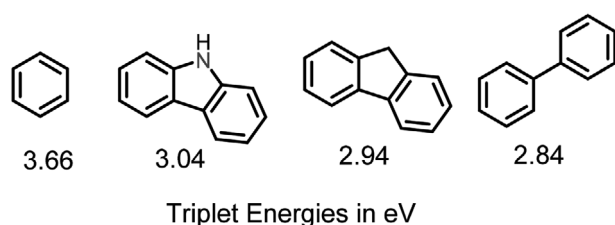


**Figure 1.** Commonly used rigid aromatic moieties for high triplet energy host materials. The triplet energies for these materials are taken from ref. [40].

occur principally on the dopant. Achieving proper HOMO and LUMO energies in the host is important as most blue phosphors are formed by stabilizing the HOMO or destabilizing the LUMO energy of a green phosphor, making hosts used for green PHOLEDs impractical for blue PHOLEDs. For example, LUMO energies in blue Ir dopants with carbene<sup>[41–43]</sup> and five-membered heterocyclic rings<sup>[44,45]</sup> are destabilized by 0.5 eV or more from values in green phosphors. Such large changes in the HOMO and/or LUMO energies can promote the formation of unwanted exciplexes between the dopants and many of the conventional hosts used in blue PHOLEDs. Therefore, a host with a wide HOMO–LUMO gap is needed to frustrate exciplex formation between the blue dopant and host.

An additional weakness in existing host materials for blue dopants is that chemical bonds in the hosts are susceptible to rupture during device operation. Energies of excitons formed in blue PHOLEDs are between 2.8 and 3.0 eV. Common building blocks in existing hosts, such as carbazole, phosphine oxide, or sulfone, have C–N, C–P, or C–S bonds, and their homolytic bond dissociation energies (BDE) tend to be close to or lower than 3.0 eV.<sup>[46]</sup> Therefore, cleavage of C–N, C–P, or C–S bonds in the excited state leads to the formation of nonradiative recombination centers and/or luminescence quenchers which degrade the device performance.

To mitigate the possibility of C–X bond rupture, research groups have investigated hydrocarbon host materials based on spiro fluorene oligomers<sup>[47–51]</sup> and polymers<sup>[52,53]</sup> that utilize C–C linkages with a BDE of  $\approx 3.6$  eV.<sup>[54]</sup> Unfortunately, their triplet energies are relatively low ( $E_T \leq 2.8$  eV) in solution owing to  $\pi$  conjugation between covalently linked phenyl rings. As shown in Figure 1, fluorene has a triplet energy of 2.94 eV. Therefore, linking the spirofluorene units together into oligomers and polymers, while increasing the glass transition temperature ( $T_g$ ), also causes a corresponding decrease in triplet energies.<sup>[46–52]</sup>

To obtain compounds with high triplet energies, our previous work bypassed molecules with direct phenyl–phenyl linkages and instead employed materials, termed ultrawide gap hosts (UGH), where individual phenyl rings are bound to a tetravalent silicon core atom, e.g. 1,4-(Ph<sub>3</sub>Si)C<sub>6</sub>H<sub>4</sub>(SiPh<sub>3</sub>).<sup>[55]</sup> This approach electronically isolates the arene rings in the molecule and leads to high triplet energies ( $E_T > 3.2$  eV). Exciton formation in UGH-based OLEDs occurs by charge recombination at the phosphorescent emitter, achieving high external efficiency, while avoiding exciplex formation between the guest and host.<sup>[19]</sup> Unfortunately, UGH-type materials often

have low glass transition temperatures, which limit the stability of OLEDs that incorporate them as hosts. Replacing the central phenylene group in UGHs with a biphenyl linkage increases the  $T_g$ , however, the triplet energy of such modified hosts drops to 2.7 eV in solution.<sup>[56]</sup> These trade-offs between enhancing the glass transition temperature and minimizing electronic conjugation present another challenge to the design of host materials for blue phosphors.

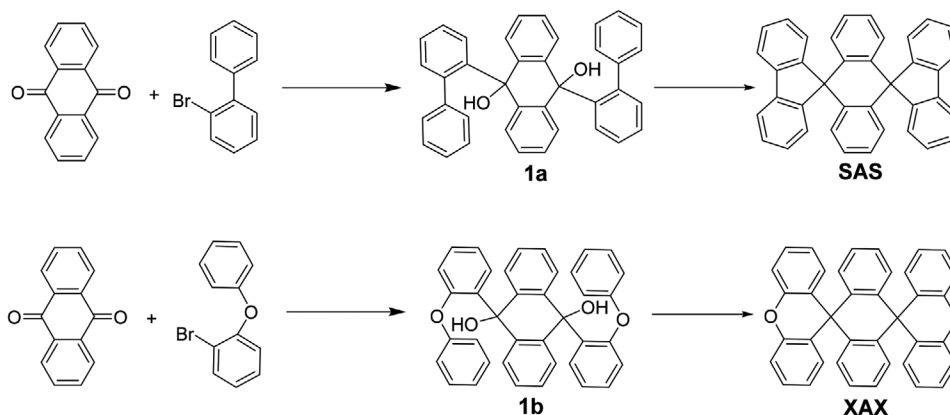
In this work, we aim to build host molecules with high energy gaps, strong covalent linkages and good thermal stability. Here we focus on spiro-based materials to achieve high thermal stability.<sup>[57]</sup> Our study also involves a comparison of the properties of a host with biphenylene groups to one with isolated phenyl rings. To that end, two building blocks, fluorene and benzene (Figure 1), are linked together via double spiro centers on a dihydroanthracene core to form dispiro[fluorene-9,9'-anthracene-10',9''-fluorene] (SAS) and dispiro[xanthene-9,9'-anthracene-10',9''-xanthene] (XAX). As the fluorene and phenyl units are isolated by spiro centers, SAS and XAX maintain high triplet energies not only in solution ( $E_T = 2.92$  and 3.44 eV, respectively) but also in solid state ( $E_T = 2.77$  and 3.08 eV, respectively). Both compounds also have large energy separations between their respective HOMOs and LUMOs ( $\geq 5.0$  eV). Furthermore, SAS and XAX only have C–C or comparably strong C–O bonds and are stable up to 450 °C. SAS and XAX have been successfully used as host materials to fabricate blue PHOLEDs with a low turn-on voltage ( $\approx 2.9$  V) and high external quantum efficiency (EQE = 18% and 16% at 0.01 mA cm<sup>-2</sup>, respectively).

## 2. Results and Discussion

### 2.1. Synthesis and Structures

SAS and XAX were synthesized from readily available starting materials in high yields using a two-step sequence (**Scheme 1**). The first step in either SAS or XAX synthesis is lithiation of 2-bromobiphenyl or 1-bromo-2-phenoxybenzene with *n*-butyllithium, respectively, followed by nucleophilic addition of the anion to the anthraquinone, which gives the desired intermediates (1a and 1b) in 85% yield. The next step involves acid-mediated Friedel–Crafts cyclization of the hydroxyl precursors, giving the desired products in 80% yield.

The crystal structures of SAS and XAX are shown in **Figure 2**. The spiro linkages prevent electronic interaction between the  $\pi$ -systems on either side of the spiro linkage in both SAS and XAX. The spirofluorene planes of SAS are nearly perpendicular to the plane of dihydroanthracene (dihedral angle = 87°). Unlike the spirofluorene groups of SAS, the two arenes of the diaryl-ether moiety in XAX are not coplanar. The dihedral angle between the two arene rings, illustrated by the two-colored planes in Figure 2, is 11° and 18° for the two independent XAX molecules in the unit cell. The closest intermolecular contacts observed in crystals involve face-to-edge packing, with shortest C...C spacings of 3.70 and 3.80 Å between dihydroanthracene aryl planes and the edges of the fluorene or diaryl-ether in SAS and XAX, respectively (see Figures S1 and S2, Supporting Information). No close face-to-face contacts



**Scheme 1.** Synthesis of SAS and XAX.

are observed between the  $\pi$ -systems of adjacent molecules in crystals of either compound.

The electronic structure, valence molecular orbital compositions, and energies, along with the triplet excited state energies (Figure 3) were examined theoretically using density functional theory (DFT) at the B3LYP/6-31G\*\* level of theory. The structural parameters of the geometry optimized compounds compare well with data obtained from the single-crystal X-ray analysis. The dihedral angle between spirofluorene and dihydroanthracene in SAS is  $90^\circ$  in the optimized structure, close to the value observed in the single crystal. The dihedral angle between the planes of the two flanking aromatic rings in XAX is  $15^\circ$ , intermediate between those observed in the crystal structure. The HOMO/LUMO contours of SAS are primarily localized on the biphenyl moieties resulting in a large energy gap, whereas the triplet spin density is localized on a single biphenyl moiety (the HOMO, LUMO, and triplet spin density were predicted using DFT calculations, see the Experimental section for details). The HOMO of XAX is mainly localized on aryl-ether moieties whereas the LUMO is delocalized over every aromatic ring in the molecule. The calculated energies for the HOMO and LUMO of XAX are similar to those of SAS. The triplet state has a spin density that is distributed principally over one aromatic ring in XAX and has a high energy ( $E_T = 3.54$  eV).

## 2.2. Photophysical, Electrochemical and Thermal Properties

Absorption spectra of SAS and XAX recorded in 2-methyltetrahydrofuran (2-MeTHF) are shown in Figure 4a. SAS and XAX display absorption bands between 250 and 350 nm, where the peak at lowest energy is attributed a  $\pi$  to  $\pi^*$  transitions on the flanking arene rings. The fluorescence spectra of SAS and XAX in 2-MeTHF at room temperature are featureless and exhibit a Stokes shift of  $\approx 1600$   $\text{cm}^{-1}$  (Figure 4b). Singlet energies for SAS ( $E_S = 3.96$  eV) and XAX ( $E_S = 4.26$  eV) were determined from the onset of the fluorescence spectra. The phosphorescence spectra of the compounds were measured in 2-MeTHF (Figure 4c) and as neat solids (Figure 4d) at 77 K. The triplet energy of SAS estimated from the onset of the phosphorescent spectrum ( $E_T = 2.92$  eV) is redshifted in the solid state ( $E_T = 2.77$  eV). Isolation of aromatic rings in XAX leads to triplet energies in solution ( $E_T = 3.44$  eV) and in the solid state ( $E_T = 3.08$  eV) that are markedly higher values found for SAS (Table 1). Triplet energies of SAS and XAX measured in solution agree with calculated values, whereas the triplet energies measured in solid state are lower due to effects from aggregation.

Electrochemical properties of SAS and XAX were determined by cyclic voltammetry (CV) and differential pulse voltammetry (DPV) (Figure S3, Supporting Information).

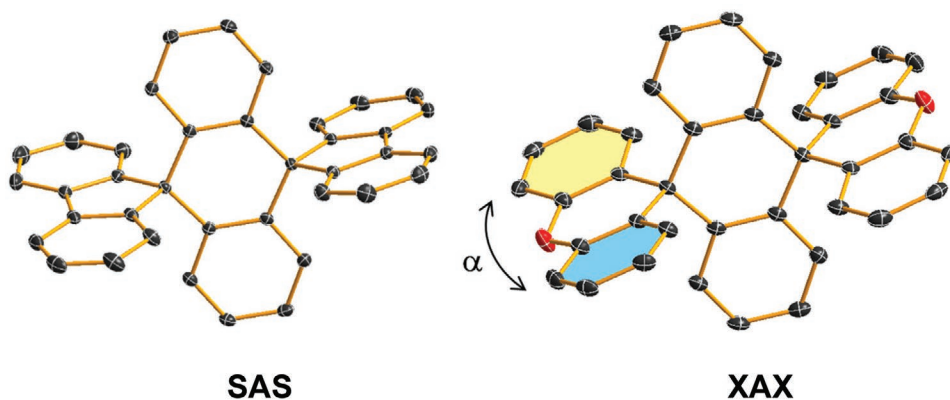


**Figure 2.** Crystal structures of SAS and XAX with thermal ellipsoids at 50%. Hydrogen atoms were omitted for clarity.  $\alpha$  is the angle between yellow and blue colored arene rings in XAX.

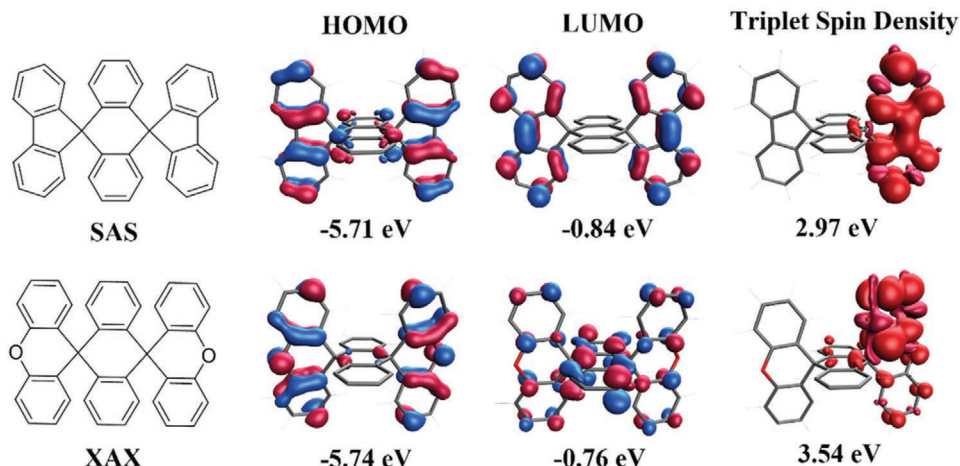


**Figure 3.** Frontier molecular orbitals and triplet spin density calculated for SAS and XAX (B3LYP/6-31G\*\*).

Oxidation potentials of compounds were determined by using decamethylferrocene (DMFc) as an internal reference and are reported relative to the ferrocenium/ferrocene ( $\text{Fc}^+/\text{Fc}$ ) redox couple. SAS and XAX display irreversible oxidation waves near 1.05 V in acetonitrile (MeCN). HOMO energies estimated from their respective oxidation potentials ( $-6.0$  eV for both SAS and XAX) agree well with values obtained using ultraviolet photoelectron spectroscopy (UPS,  $-5.9$  eV for SAS and  $-6.3$  eV for XAX) (Figure S4, Supporting Information). The reduction potentials of both SAS and XAX lie beyond the potential of the MeCN solvent ( $-3.0$  V), indicating a LUMO level for these

materials shallower than  $-1$  eV (LUMO =  $-1.18 \times E_{\text{red}} - 4.83$ ).<sup>[58]</sup> Therefore, the HOMO-LUMO gaps of SAS and XAX derived from UPS and electrochemical studies are greater than 5.0 eV. Overall, compared to the widely used host 3,3'-bis(carbazol-9-yl) biphenyl (*m*CBP), SAS and XAX have higher triplet energies and larger HOMO-LUMO gaps (Table 1).

The thermal properties of SAS and XAX were investigated using thermogravimetric analysis (TGA, Table 1). Both compounds are thermally stable up to 450 °C. No decomposition was observed before the sublimation of these materials in TGA experiments (Figure S5, Supporting Information). Likewise, no

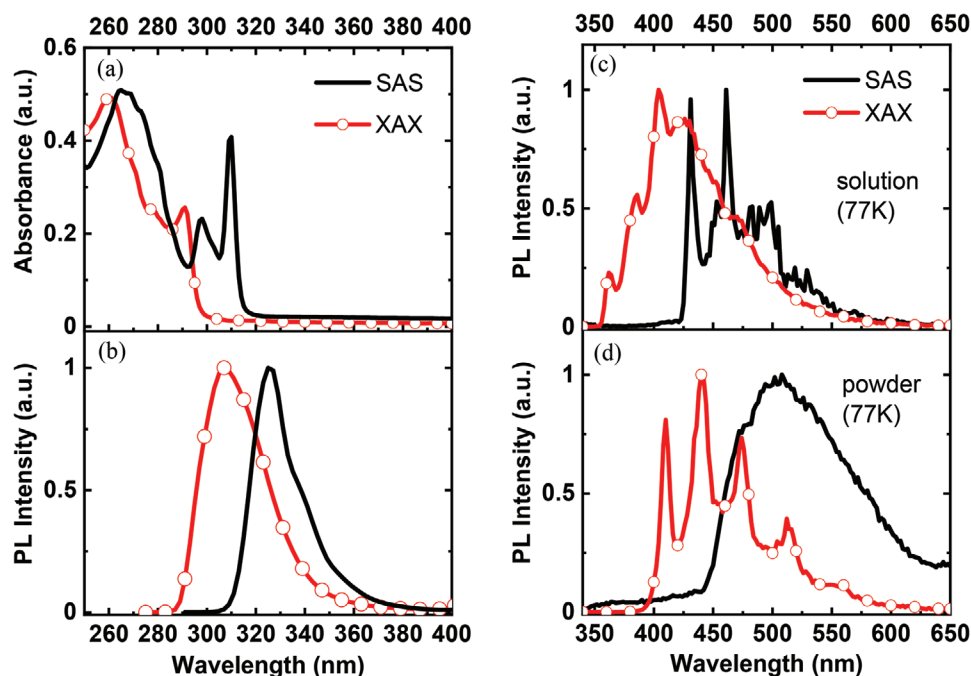


**Figure 4.** a) Absorption and b) emission spectra of SAS and XAX in 2-MeTHF at 298 K. Gated emission (phosphorescence) spectra of SAS and XAX at 77 K are shown for samples in c) 2-MeTHF solutions and d) as neat solids. The spectra for (c) and (d) were collected with a time delay of 200  $\mu\text{s}$ . SAS emission spectra were excited at 290 nm and XAX emission spectra were excited at 275 nm.



**Table 1.** Summary of properties of SAS and XAX.

	Abs [eV] <sup>a)</sup>	S <sub>1</sub> [eV] <sup>a)</sup>	T <sub>1</sub> [eV] <sup>b)</sup>	T <sub>1</sub> [eV] <sup>c)</sup>	E <sub>ox</sub> [V] <sup>d)</sup>	HOMO [eV] <sup>e)</sup>	HOMO [eV] <sup>f)</sup>	T <sub>g</sub> [°C] <sup>g)</sup>
SAS	4.00	3.96	2.92	2.77	1.05	-6.0	-5.9	409
XAX	4.27	4.26	3.44	3.08	1.03	-6.0	-6.3	417
mCBP <sup>h)</sup>	–	3.60	2.93	2.86	0.88	-5.8	–	–

<sup>a)</sup>Peak of the absorption band and onset of the fluorescence measured in 2-MeTHF at 298 K; <sup>b)</sup>Onset of the phosphorescence band measured in 2-MeTHF at 77 K; <sup>c)</sup>Onset of the phosphorescence band for the neat powder at 77 K; <sup>d)</sup>Obtained using DPV in acetonitrile versus Fc<sup>+</sup>/Fc; <sup>e)</sup>Calculated from equation (HOMO = -1.15 × E<sub>ox</sub> - 4.79) according to ref. [58] with redox potentials adjusted versus ferrocene as 0 V. The redox potential measured for decamethylferrocene relative to ferrocene can be found in the experimental section; <sup>f)</sup>Obtained using UPS; <sup>g)</sup>T<sub>g</sub> = sublimation temperature under nitrogen; <sup>h)</sup>Data from ref. [32].

glass transition or melting temperature was observed for SAS and XAX solids upon analysis using differential scanning calorimetry (DSC). The high thermal and morphological stability of the compounds is ascribed to the rigid double spiro configuration in the molecular structure.

### 2.3. Electroluminescent Properties

The performance of SAS and XAX as host materials was investigated by fabricating vacuum-deposited films (80 nm thick) using a blue-emitting phosphor we recently reported, *fac*-tris(N,N-di-*p*-tolyl-pyridinoimidazol-2-yl)iridium(III) (Ir(tpz)<sub>3</sub>)<sup>[59]</sup> as a dopant across a range of concentrations. The molecular structure of Ir(tpz)<sub>3</sub> is shown in **Figure 5**. This Ir dopant was chosen for study because it has high chemical and thermal stability and excellent photophysical properties, parameters which are crucial for fabricating efficient PHOLEDs. Moreover, the ligand in Ir(tpz)<sub>3</sub> is a cyclometalated N-heterocyclic carbene, Ir(C<sup>^</sup>C)<sub>3</sub>. Blue phosphors using these types of ligands have an advantage over traditional Ir complexes using C<sup>^</sup>N: ligands as they do not have datively bound nitrogen groups such as Ir-pyridyl, which are prone to bond rupture in the excited state.<sup>[60–62]</sup>

The photoluminescence quantum yields (Φ<sub>PL</sub>), emission lifetimes (τ), and decay rates of the films as a function of Ir(tpz)<sub>3</sub> doping level in SAS and XAX are summarized in **Table 2**. The films give sole emission from Ir(tpz)<sub>3</sub> at doping levels ≥10 vol% (Figure S6, Supporting Information). The Φ<sub>PL</sub> of SAS films containing 20–30 vol% Ir(tpz)<sub>3</sub> are close to 100% and have non-radiative rates (k<sub>nr</sub>) an order of magnitude lower compared to 10 vol% film. In contrast, the Φ<sub>PL</sub> in XAX films drops as Ir(tpz)<sub>3</sub> concentration increases to 30 vol% due to an increase in k<sub>nr</sub>. These results suggest that both SAS and XAX confine excitons on the blue phosphor, with the dopant being less effectively dispersed in XAX at high concentration.

PHOLEDs using Ir(tpz)<sub>3</sub> as a dopant were fabricated in SAS and XAX hosts. The performance of these devices was compared to reference devices fabricated with a commonly used host in blue OLEDs, mCBP, see **Table 3**. In the first set of experiments, devices were analyzed using different concentrations of Ir(tpz)<sub>3</sub> doped in SAS, XAX, and mCBP (see Figures S8–S10, Supporting Information for the OLED performance). In SAS-based PHOLEDs, the current density (J) increased as the doping level was raised from 10% to 30%. The turn-on voltage (V<sub>on</sub>, defined at brightness of 1 cd m<sup>-2</sup>) dropped from 3.15 to 2.80 V over the same range. The increase in current density with doping concentration is consistent with charges being injected directly onto

and carried by the dopant, as expected since the energies of the HOMO and LUMO for Ir(tpz)<sub>3</sub> (-5.6 and -2.0 eV, respectively) are nested within those of SAS (Figure 5). The same trend of current density increasing with doping concentration is observed in XAX-based devices. However, J decreases with increasing doping concentration in devices using the mCBP host. This difference is likely due to mCBP carrying both holes and electrons at low doping concentration since the energies of its HOMO (-5.8 eV) and LUMO (-1.6 eV) are close to those of Ir(tpz)<sub>3</sub>.<sup>[63–65]</sup> In contrast, charges are exclusively trapped and transported by Ir(tpz)<sub>3</sub> in SAS and XAX films since both materials have deeper HOMO and shallower LUMO levels.

The electroluminescence (EL) spectra of Ir(tpz)<sub>3</sub> in SAS, XAX and mCBP hosts match the PL spectra of Ir(tpz)<sub>3</sub> (Figure 5a). The EL spectrum is similar in all host materials, with minor differences presumably due to optical cavity effects. The SAS and XAX based devices have the same turn-on potential (≈2.9 V) and have similar current–voltage (J–V) characteristics, whereas the SAS device is slightly more conductive (Figure 5b). The XAX and reference host mCBP devices exhibit similar brightness at low current densities, with slight differences at higher current densities. PHOLEDs with SAS give the highest efficiency (EQE = 18%) whereas the XAX device has a slightly lower efficiency (EQE = 16%) (Figure 5c). The SAS-based devices remain efficient (EQE ≈ 10%) at high brightness (10 000 cd m<sup>-2</sup>), whereas the EQEs of XAX based devices drop dramatically at >1000 cd m<sup>-2</sup>. This difference suggests that SAS avoids aggregation-induced quenching of the long-lived triplet excitons as is observed in UGH-type hosts.<sup>[55]</sup>

### 3. Conclusion

We report two wide energy gap hosts without heteroatomic exocyclic bonds. SAS and XAX have been prepared in high yields, from readily available precursors. The double spiro structure in SAS and XAX interrupts conjugation between aromatic π systems by holding the spirofluorene or diphenylether moieties orthogonal to the dihydroanthracene core. As a result, both SAS and XAX have large HOMO–LUMO gaps (≥5.0 eV) and, more importantly, retain high triplet energies (E<sub>T</sub> = 2.77 and 3.08 eV, respectively) in the solid state, parameters which are crucial in hosting blue phosphors. XAX has a higher triplet energy than that of SAS due to isolated phenyl rings in diphenyl ether moieties, showing that the high triplet energy of the fluorene group limits the applicability of SAS as a host for deep blue phosphors. The high thermal stabilities of SAS and XAX

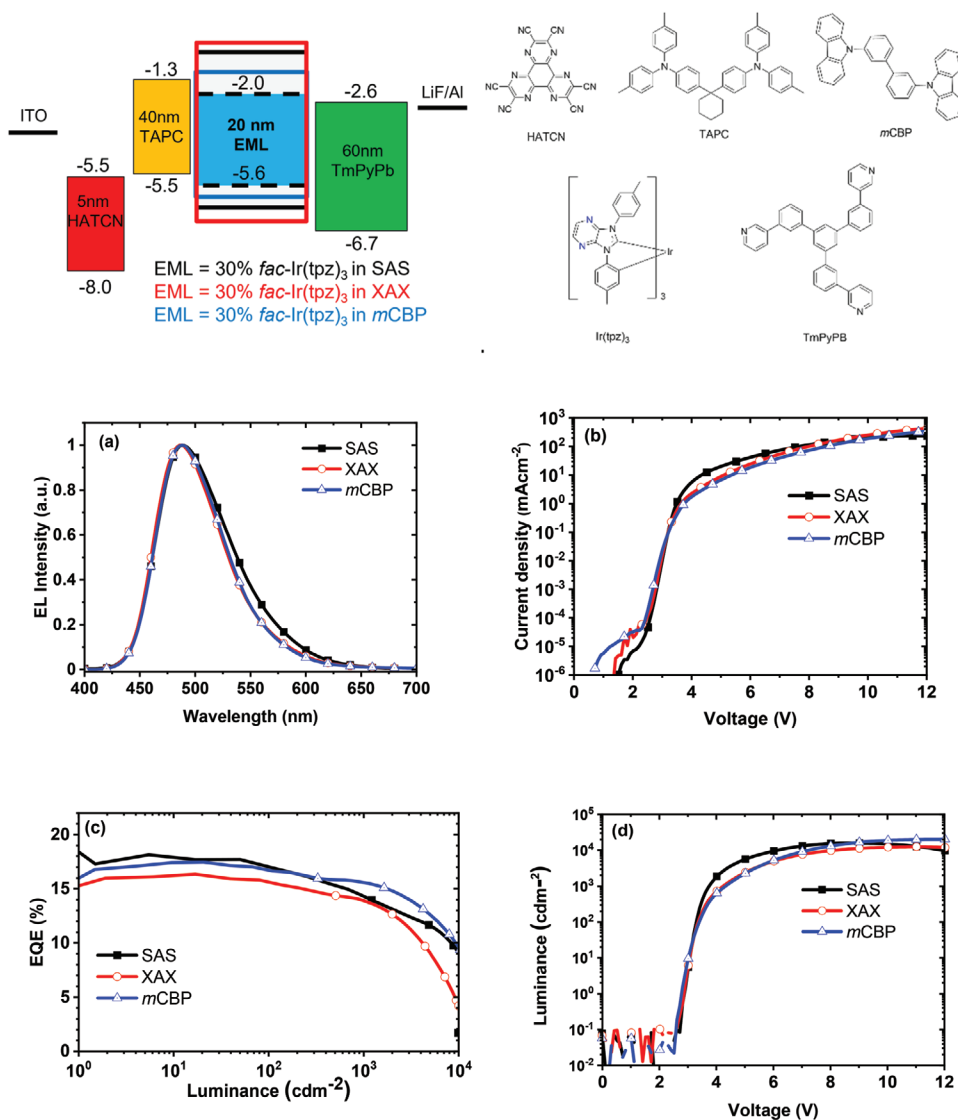


**Figure 5.** OLED device characteristics of SAS, XAX and *mCBP*. (top) Device architecture and molecular structure of materials. a) EL spectra. b) *J*–*V* curves. c) Efficiency versus luminance curves. d) Luminance versus voltage curves.

**Table 2.** Summary of photoluminescence properties for Ir(tpz)<sub>3</sub> doped into SAS and XAX films.

Concentration [%]	$\Phi_{\text{PL}}$ [%, $\sigma$ ]	$\tau$ [ $\mu\text{s}$ , $\sigma$ ] <sup>c)</sup>	$k_{\text{r}}$ [10 <sup>5</sup> s <sup>-1</sup> ]	$k_{\text{nr}}$ [10 <sup>5</sup> s <sup>-1</sup> ]
in SAS				
10	87, 2 <sup>a)</sup>	1.37, 0.06	6.4	1.0
20	97, 2 <sup>a)</sup>	1.53, 0.05	6.3	0.2
30	98, 2 <sup>a)</sup>	1.47, 0.02	6.7	0.1
in XAX				
10	93, 2 <sup>b)</sup>	1.43, 0.07	6.5	0.5
20	91, 2 <sup>b)</sup>	1.42, 0.04	6.4	0.6
30	86, 2 <sup>b)</sup>	1.27, 0.05	6.8	1.1

<sup>a)</sup> Measured with excitation energy at 310 nm; <sup>b)</sup> Measured with excitation energy at 290 nm. Quantum yield is the average of four measurements, listed with their standard deviation ( $\sigma$ ); <sup>c)</sup> Measured at emission at 490 nm. Lifetime is the average of three measurements, listed with their standard deviation ( $\sigma$ ). Decay traces and fits are shown in Figure S7 (Supporting Information).

**Table 3.** OLED performance parameters for Ir(tpz)<sub>3</sub> based OLEDs.

Host	V <sub>on</sub> [V]	EQE <sub>max</sub> [%;σ]	Efficiency at 1000 cd m <sup>-2</sup>				λ <sub>max</sub> [nm] (CIE)
			EQE [%]	Current density [mA cm <sup>-2</sup> ]	CE [cd A <sup>-1</sup> ]	PE [lm W <sup>-1</sup> ]	
SAS <sup>a)</sup>	2.9	17.9, 0.2 <sup>b)</sup>	14	2.62	35	30	488 (0.19, 0.40)
XAX	2.9	15.7, 0.4 <sup>b)</sup>	14	3.19	31	23	488 (0.17, 0.37)
mCBP	2.8	17.1, 0.1 <sup>c)</sup>	15	2.79	35	26	488 (0.17, 0.38)

<sup>a)</sup>V<sub>on</sub> = voltage at 1 cd m<sup>-2</sup>; EQE<sub>max</sub> = EQE at 0.01 mA cm<sup>-2</sup>, L = luminance, CE = current efficiency, PE = power efficiency; <sup>b)</sup>Maximum EQE is the average of four devices, listed with their standard deviation (σ); <sup>c)</sup>Maximum EQE is the average of two devices.

are attributed to double spiro centers on the dihydroanthracene core. We utilized these wide energy gap materials as hosts for a blue phosphor to fabricate bright, efficient blue PHOLEDs. The SAS and XAX compounds act as inert matrices that enable guest dopants to directly transport and trap charges that subsequently form excitons, which lead to high-performance devices. These compounds can serve as platforms on which to build other high-energy host materials.

## 4. Experimental Section

**Synthesis and Characterization:** All commercial reagents and solvents are purchased from Sigma Aldrich or Matrix Scientific and used without further purification. All reactions were carried out using standard Schlenk line techniques, using dried and degassed solvents. The synthesis of SAS and XAX was modified from a literature method for related compounds.<sup>[66]</sup> A key modification from the literature procedure was preparation of 1a using *n*-butyllithium (*n*-BuLi) instead of a Grignard reagent which gave the product in higher yield. Iridium (III)*N,N*-di-*p*-tolyl-pyridinoimidazol-2-yl was prepared as previously.<sup>[59]</sup> <sup>1</sup>H NMR spectra were recorded on a Varian 400 instrument. <sup>13</sup>C NMR spectrum was recorded on a Varian 600 instrument. Mass spectra were recorded on a Bruker Auto Flex Speed Laser Desorption Ionization (LDI) Mass Spectrometer. Elemental analyses were performed using a Thermo Scientific FlashSmart CHNS elemental analyzer.

**9,10-Di([1,1'-biphenyl]-2-yl)-9,10-dihydroanthracene-9,10-diol (1a):** Dry and degassed THF was cannula transferred into a nitrogen-purged 250 mL round bottom flask. 2-Bromobiphenyl (2.48 mL, 14.4 mmol, 2 eq.) was added and the solution was cooled to -78 °C. *n*-BuLi (6.34 mL, 2.5 M, 2.2 eq.) was added dropwise. After 1 h of stirring at -78 °C, a solution of anthraquinone (1.5 g, 7.2 mmol, 1.00 eq.) in 15 mL of THF was added to the mixture over 5 min. The reaction mixture warmed up to room temperature over a period of 8 h and stirred overnight. The resulting mixture was quenched with water (30 mL), yielding an off-white solid. The mixture was transferred to a Büchner funnel and vacuum filtered. The residue was washed with ether resulting in a white powder. Yield: 3.2 g, 86%. <sup>1</sup>H NMR (400 MHz, Chloroform-*d*, δ): 8.45 (dd, *J* = 8.1, 1.3 Hz, 2H; Ar H), 7.48 (ddd, *J* = 8.1, 1.5 Hz, 2H; Ar H), 7.24 (dd, *J* = 7.4, 1.3 Hz, 2H; Ar H), 7.17–7.10 (m, 6H; Ar H), 6.95 (dd, *J* = 6.1, 3.4 Hz, 4H; Ar H), 6.87 (tt, *J* = 8.1, 1.5 Hz, 4H; Ar H), 6.70 (dd, *J* = 7.5, 1.5 Hz, 2H; Ar H), 5.93 (dd, *J* = 8.1, 1.3 Hz, 4H; Ar H). [M-2OH] calcd for C<sub>38</sub>H<sub>26</sub>, 482.2; found, 482. 6.

**9,10-Bis(2-phenoxyphenyl)-9,10-dihydroanthracene-9,10-diol (1b):** Dry and degassed THF was cannula transferred into a nitrogen purged 250 mL round bottom flask. 1-Bromo-2-phenoxybenzene (4.79 g, 19.21 mmol, 2 eq.) was added and the solution was cooled down to -78 °C. *n*-BuLi (8.45 mL, 2.5 M, 2.2 eq.) was added dropwise. After 1 h of stirring at -78 °C, a solution of anthraquinone (2 g, 9.61 mmol, 1.00 eq.) in 20 mL of THF was added to the mixture over 5 min. The reaction mixture warmed up to room temperature over a period of 8 h and stirred overnight. The resulting mixture was quenched with water (30 mL), yielding an off-white solid. The mixture was transferred to a Büchner funnel and vacuum filtered. The residue was washed with ether resulting

in a white powder. Yield: 4.5 g, 85%. <sup>1</sup>H NMR (400 MHz, Chloroform-*d*, δ): 8.36 (dd, *J* = 7.8, 1.8 Hz, 2H; Ar H), 7.23–7.10 (m, 12H; Ar H), 7.05 (tdd, *J* = 7.8, 1.8 Hz, 4H; Ar H), 6.94 (tt, *J* = 7.2, 1.8 Hz, 2H; Ar H), 6.47 (dd, *J* = 8.0, 1.3 Hz, 2H; Ar H), 6.17 (dd, *J* = 8.7, 1.3 Hz, 4H; Ar H). MS: [M-2OH] calcd for C<sub>38</sub>H<sub>26</sub>O<sub>2</sub>, 514.2; found, 514.5.

**Dispiro[fluorene-9,9'-anthracene-10',9'-fluorene] (SAS):** The resulting solid 1a (3.2 g, 6.19 mmol, 1 eq.) was dissolved in a mixture of solution of 106 mL (1.86 mol, 300 eq.) glacial acetic acid and 15.5 mL (12 M, 30 eq.) hydrochloric acid. The reaction was stirred for 12 h at 110 °C under reflux. The reaction mixture was cooled to room temperature, filtered, and washed with DI water yielding a white solid. Yield: 2.5 g, 84%. The compound was further purified by sublimation at 270 °C and 10<sup>-6</sup> torr. <sup>1</sup>H NMR (400 MHz, Acetone-*d*<sub>6</sub>, δ): 8.07 (ddd, *J* = 7.5, 1.0 Hz, 4H; Ar H), 7.47 (ddd, *J* = 7.5, 1.5 Hz, 4H; Ar H), 7.36–7.28 (m, 8H; Ar H), 6.83 (dd, *J* = 6.1, 3.4 Hz, 4H; Ar H), 6.35 (dd, *J* = 6.1, 3.4 Hz, 4H; Ar H). <sup>13</sup>C NMR (151 MHz, Chloroform-*d*, δ): 157.51, 140.67, 136.53, 128.95, 128.68, 127.66, 126.91, 125.63, 120.24, 58.13. Anal. calcd for C<sub>38</sub>H<sub>24</sub>: C 94.97, H 5.03; found: C 94.95, H 5.06. MS: [M] calcd for C<sub>38</sub>H<sub>24</sub>, 480.2; found, 480.4.

**Dispiro[xanthene-9,9'-anthracene-10',9'-xanthene] (XAX):** The resulting solid 1b (4.5 g, 8.2 mmol, 1 eq.) was dissolved in a mixture of solution of 140 mL (2.46 mol, 300 eq.) glacial acetic acid and 20.5 mL (12 M, 30 eq.) hydrochloric acid. The reaction mixture was stirred for 12 h at 110 °C under reflux. The reaction mixture was cooled to room temperature, filtered, and washed with DI water yielding a white solid. Yield: 3.5 g, 83%. The compound was further purified by sublimation at 290 °C and 10<sup>-6</sup> torr. <sup>1</sup>H NMR (400 MHz, Chloroform-*d*, δ): 7.29 (dd, *J* = 8.2, 1.5 Hz, 4H; Ar H), 7.23 (ddd, *J* = 8.2, 1.5 Hz, 4H; Ar H), 7.11 (dd, *J* = 6.1, 3.4 Hz, 4H; Ar H), 6.98 (dd, *J* = 6.1, 3.4 Hz, 4H; Ar H), 6.93 (ddd, *J* = 8.0, 1.5 Hz, 4H; Ar H), 6.87 (dd, *J* = 8.2, 1.5 Hz, 4H; Ar H). Anal. calcd for C<sub>38</sub>H<sub>24</sub>O<sub>2</sub>: C 89.04, H 4.72; found: C 88.68, H 4.77. MS: [M] calcd for C<sub>38</sub>H<sub>24</sub>O<sub>2</sub>, 514.2; found, 514.5.

**Electrochemical, Physical, and Photophysical Measurements:** Cyclic voltammetry (CV) and differential pulse voltammetry (DPV) were performed in MeCN using a VersaSTAT 3 potentiostat with a 0.1 M tetra-*n*-butyl ammonium hexafluorophosphate (TBAF) as the supporting electrolyte, an Ag wire was used as the pseudo reference electrode, a Pt wire as the counter electrode, and a glassy carbon rod as the working electrode. Decamethylferrocene is employed as an internal reference. To determine the relative redox potential of decamethylferrocene compared to ferrocene, CV and DPV scans are performed with these two references only as shown in Figure S3 (Supporting Information). Two references present reversible oxidation peaks as shown in CV plots. According to the DPV results, when the redox potentials of ferrocene are fixed to 0.0 V, those of decamethylferrocene are around -0.54 V. Thus, by setting the decamethyl ferrocene reference peaks at -0.54 V, all the samples' redox potentials are reported relative to 0.0 V for ferrocene. The redox potentials of SAS and XAX are based on the values from differential pulsed voltammetry measurements and are reported relative to the Fc<sup>+</sup>/Fc redox couple, whereas cyclic voltammetry was measured to look at if any electrochemical reversibility is inherent to these materials in order to obtain more accurate redox potentials.

Ultraviolet photoelectron spectroscopy was carried out with a He I UV source that has a photon energy of 21.2 eV under high vacuum

( $10^{-8}$  torr). The spectra were collected by a hemispherical electron energy analyzer (Thermal VG) with a  $-8.0$  V bias voltage. Thermogravimetric analysis (TGA) measurements were performed on a NETZSCH STA 449F3 thermogravimeter under nitrogen at a heating rate of  $10$  °C  $\text{min}^{-1}$ .

UV–vis absorption spectra were recorded using a Hewlett-Packard 8453 diode array spectrometer. Steady-state photoluminescent emission spectra were performed using a Photon Technology International QuantaMaster model C-60 fluorimeter, whereas gated photoluminescent emission spectra were measured on the same instrument using a Xe flash lamp with  $200$   $\mu\text{s}$  delay. Photoluminescent quantum yields were determined using a Hamamatsu C9920 system equipped with a Xe lamp, calibrated integrating sphere and model C10027 photonic multichannel analyzer (PMA). Solution samples were deoxygenated by bubbling  $\text{N}_2$  in a quartz cuvette fitted with a Teflon stopcock. Powder samples were measured in a quartz NMR tube. Films were prepared by vacuum deposition ( $10^{-7}$  Torr) on quartz substrates. Emission lifetimes were measured by time-correlated single-photon counting using an IBH Fluorocube instrument. Radiative rates are obtained from the equation  $k_r = \frac{\phi_{PL}}{\tau}$  and nonradiative rates are obtained from the equation  $k_{nr} = \frac{1 - \phi_{PL}}{\tau}$ .

The single crystals were obtained through sublimation. See the synthesis section for details of sublimation. Single crystal structures were determined at  $100$  K with Bruker X-ray diffractometer, equipped with an APEX II CCD detector and an Oxford Cryosystems 700 low temperature apparatus, using Mo  $K\alpha$  radiation. Details of the data collection and structure solution are given in the Supporting Information. CCDC 1978365 (SAS) and 1978366 (XAX) contain the supplementary crystallographic data for this paper. These data can be obtained free of charge from The Cambridge Crystallographic Data Centre via [www.ccdc.cam.ac.uk/data\\_request/cif](http://www.ccdc.cam.ac.uk/data_request/cif).

**Computational Modeling:** All calculations reported in this work were performed using the Q-Chem 5.1 software package. Ground state ( $S_0$ ) and triplet state ( $T_1$ ) geometries optimization were performed for all structures at the B3LYP/6-31G\*\* level of theory. The optimized geometries of ground-state geometries were examined by frequency analysis at the B3LYP/6-31G\*\* level of theory. The energies of optimized geometries are local minimum energies as no negative values were found. The energies for the  $T_1$  state shown in Figure 3 were determined from the difference in energies between the optimized  $S_0$  and  $T_1$  geometries ( $\Delta\text{SCF}$  method).<sup>67</sup>

**OLED Fabrication and Testing:** Glass substrates with pre-patterned,  $2$  mm wide indium tin oxide (ITO) stripes were cleaned by sequential sonication in deionized water, acetone, and isopropanol, followed by  $10$  min UV ozone exposure. Organic materials and metals were deposited at rates of  $0.5$ – $2$  Å  $\text{s}^{-1}$  through shadow masks in a vacuum thermal evaporator with a base pressure of  $10^{-7}$  Torr. A separate shadow mask was used to deposit  $1$  mm wide stripes of  $100$  nm thick Al films perpendicular to the ITO stripes to form the cathode, resulting in a  $4$  mm<sup>2</sup> device area. The device structure is: glass substrate/70 nm ITO/5 nm dipyrzino [2,3-f:2',3'-h] quinoxaline-2,3,6,7,10,11-hexacarbonitrile (HATCN)/40 nm 4,4'-cyclohexylidene-bis [N,N bis(4 methylphenyl)benzenamine] (TAPC)/30 vol% fac-iridium(III)N,N-di-p-tolyl-pyridinoimidazol-2-yl (Ir(tpz)<sub>3</sub>):Host/60 nm 1,3,5-Tri(m-pyridin-3-ylphenyl)benzene (TmPyPb)/1 nm lithium fluoride (LiF)/100 nm Al. The host is either 3,3'-di(9H-carbazole-9-yl)-1,1'-biphenyl (mCBP), or one of the SAS and XAX compounds.

A semiconductor parameter analyzer (HP4156A) and a calibrated large area photodiode that collected all light exiting the glass substrate were used to measure the current density–voltage–luminance ( $J$ – $V$ – $L$ ) characteristics. The device spectra were measured using a fiber-coupled spectrometer.

## Supporting Information

Supporting Information is available from the Wiley Online Library or from the author.

## Acknowledgements

This work was supported by the Universal Display Corporation. Also, S.R.F. acknowledges the US Air Force Office of Scientific Research, Grant No. 17RT0908 for partial support of this work. The authors thank Dr. Joanna M. Guerrero for help with the TGA measurements.

## Conflict of Interest

Two of the authors (Forrest and Thompson) have a financial interest in the Universal Display Corporation, one of the founders of this study.

## Data Availability Statement

Research data are not shared.

## Keywords

blue phosphorescent organic light-emitting diodes, high triplet energy, host materials, spiro-containing materials, wide energy gap

Received: September 11, 2021

Revised: October 6, 2021

Published online: November 16, 2021

- [1] C. W. Tang, S. A. VanSlyke, *Appl. Phys. Lett.* **1987**, *51*, 913.
- [2] M. A. Baldo, S. Lamansky, P. E. Burrows, M. E. Thompson, S. R. Forrest, *Appl. Phys. Lett.* **1999**, *75*, 4.
- [3] M. Hack, M. S. Weaver, J. J. Brown, *SID Symp. Dig. Tech. Pap.* **2017**, *48*, 187.
- [4] C. Murawski, K. Leo, M. C. Gather, *Adv. Mater.* **2013**, *25*, 6801.
- [5] S. C. Xia, R. C. Kwong, V. I. Adamovich, M. S. Weaver, J. J. Brown, *IEEE 45th Annual International Reliability Physics Symposium* **2007**, 253.
- [6] F. So, D. Kondakov, *Adv. Mater.* **2010**, *22*, 3762.
- [7] C. Coburn, S. R. Forrest, *Phys. Rev. Appl.* **2017**, *7*, 041002.
- [8] S. Kim, H. J. Bae, S. Park, W. Kim, J. Kim, J. S. Kim, Y. Jung, S. Sul, S.-G. Ihn, C. Noh, S. Kim, Y. You, *Nat. Commun.* **2018**, *9*, 1211.
- [9] D. Y. Kondakov, *J. Appl. Phys.* **2007**, *102*, 114504.
- [10] N. C. Giebink, B. W. D'Andrade, M. S. Weaver, P. B. Mackenzie, J. J. Brown, M. E. Thompson, S. R. Forrest, *J. Appl. Phys.* **2008**, *103*, 044509.
- [11] K. S. Yook, J. Y. Lee, *Adv. Mater.* **2012**, *24*, 3169.
- [12] W. Song, J. Y. Lee, *Adv. Opt. Mater.* **2017**, *5*, 1600901.
- [13] J.-H. Lee, C.-H. Chen, P.-H. Lee, H.-Y. Lin, M.-k. Leung, T.-L. Chiu, C.-F. Lin, *J. Mater. Chem. C* **2019**, *7*, 5874.
- [14] Y. Wang, J. H. Yun, L. Wang, J. Y. Lee, *Adv. Funct. Mater.* **2021**, *31*, 2008332.
- [15] C. Poriel, J. Rault-Berthelot, *Adv. Funct. Mater.* **2021**, *31*, 2010547.
- [16] R. J. Holmes, S. R. Forrest, Y.-J. Tung, R. C. Kwong, J. J. Brown, S. Garon, M. E. Thompson, *Appl. Phys. Lett.* **2003**, *82*, 2422.
- [17] C. Adachi, M. A. Baldo, M. E. Thompson, S. R. Forrest, *J. Appl. Phys.* **2001**, *90*, 5048.
- [18] D. F. O'Brien, M. A. Baldo, M. E. Thompson, S. R. Forrest, *Appl. Phys. Lett.* **1999**, *74*, 442.
- [19] R. J. Holmes, B. W. D'Andrade, S. R. Forrest, X. Ren, J. Li, M. E. Thompson, *Appl. Phys. Lett.* **2003**, *83*, 3818.
- [20] S. Schmidbauer, A. Hohenleutner, B. König, *Adv. Mater.* **2013**, *25*, 2114.



- [21] D. Y. Kondakov, W. C. Lenhart, W. F. Nichols, *J. Appl. Phys.* **2007**, *101*, 024512.
- [22] S. Tokito, H. Tanaka, K. Noda, A. Okada, Y. Taga, *Appl. Phys. Lett.* **1997**, *70*, 1929.
- [23] V. I. Adamovich, M. S. Weaver, R. C. Kwong, J. J. Brown, *Curr. Appl. Phys.* **2005**, *5*, 15.
- [24] S. L. Murov, *Handbook of Photochemistry*, M. Dekker, New York **1993**.
- [25] A. van Dijken, J. J. A. M. Bastiaansen, N. M. M. Kiggen, B. M. W. Langeveld, C. Rothe, A. Monkman, I. Bach, P. Stössel, K. Brunner, *J. Am. Chem. Soc.* **2004**, *126*, 7718.
- [26] H. Inomata, K. Goushi, T. Masuko, T. Konno, T. Imai, H. Sasabe, J. J. Brown, C. Adachi, *Chem. Mater.* **2004**, *16*, 1285.
- [27] L. Zeng, T. Y. H. Lee, P. B. Merkel, S. H. Chen, *J. Mater. Chem.* **2009**, *19*, 8772.
- [28] M. M. Rothmann, S. Haneder, E. Da Como, C. Lennartz, C. Schildknecht, P. Strohrriegel, *Chem. Mater.* **2010**, *22*, 2403.
- [29] K. S. Son, M. Yahiro, T. Imai, H. Yoshizaki, C. Adachi, *Chem. Mater.* **2008**, *20*, 4439.
- [30] S.-J. Su, H. Sasabe, T. Takeda, J. Kido, *Chem. Mater.* **2008**, *20*, 1691.
- [31] M. K. Kim, J. Kwon, T.-H. Kwon, J.-I. Hong, *New J. Chem.* **2010**, *34*, 1317.
- [32] M. Idris, C. Coburn, T. Fleetham, J. Milam-Guerrero, P. I. Djurovich, S. R. Forrest, M. E. Thompson, *Mater. Horiz.* **2019**, *6*, 1179.
- [33] J. Ding, Q. Wang, L. Zhao, D. Ma, L. Wang, X. Jing, F. Wang, *J. Mater. Chem.* **2010**, *20*, 8126.
- [34] H. S. Son, C. W. Seo, J. Y. Lee, *J. Mater. Chem.* **2011**, *21*, 5638.
- [35] S. O. Jeon, K. S. Yook, C. W. Joo, J. Y. Lee, *Adv. Funct. Mater.* **2009**, *19*, 3644.
- [36] F.-M. Hsu, C.-H. Chien, P.-I. Shih, C.-F. Shu, *Chem. Mater.* **2009**, *21*, 1017.
- [37] X. Cai, A. B. Padmaperuma, L. S. Sapochak, P. A. Vecchi, P. E. Burrows, *Appl. Phys. Lett.* **2008**, *92*, 083308.
- [38] H.-H. Chou, C.-H. Cheng, *Adv. Mater.* **2010**, *22*, 2468.
- [39] R.-F. Chen, G.-H. Xie, Y. Zhao, S.-L. Zhang, J. Yin, S.-Y. Liu, W. Huang, *Org. Electron.* **2011**, *12*, 1619.
- [40] S. P. McGlynn, T. Azumi, M. Kinoshita, *Molecular Spectroscopy of the Triplet State*, Prentice-Hall, Inc., Englewood Cliffs, NJ **1969**.
- [41] R. J. Holmes, S. R. Forrest, T. Sajoto, A. Tamayo, P. I. Djurovich, M. E. Thompson, J. Brooks, Y.-J. Tung, B. W. D'Andrade, M. S. Weaver, R. C. Kwong, J. J. Brown, *Appl. Phys. Lett.* **2005**, *87*, 243507.
- [42] J. Lee, H.-F. Chen, T. Batagoda, C. Coburn, P. I. Djurovich, M. E. Thompson, S. R. Forrest, *Nat. Mater.* **2016**, *15*, 92.
- [43] K.-Y. Lu, H.-H. Chou, C.-H. Hsieh, Y.-H. O. Yang, H.-R. Tsai, H.-Y. Tsai, L.-C. Hsu, C.-Y. Chen, I.-C. Chen, C.-H. Cheng, *Adv. Mater.* **2011**, *23*, 4933.
- [44] A. B. Tamayo, B. D. Alleyne, P. I. Djurovich, S. Lamansky, I. Tsyba, N. N. Ho, R. Bau, M. E. Thompson, *J. Am. Chem. Soc.* **2003**, *125*, 7377.
- [45] S.-C. Lo, C. P. Shipley, R. N. Bera, R. E. Harding, A. R. Cowley, P. L. Burn, I. D. W. Samuel, *Chem. Mater.* **2006**, *18*, 5119.
- [46] N. Lin, J. Qiao, L. Duan, L. Wang, Y. Qiu, *J. Phys. Chem. C* **2014**, *118*, 7569.
- [47] Z. Jiang, H. Yao, Z. Zhang, C. Yang, Z. Liu, Y. Tao, J. Qin, D. Ma, *Org. Lett.* **2009**, *11*, 2607.
- [48] L. J. Sicard, H.-C. Li, Q. Wang, X.-Y. Liu, O. Jeannin, J. Rault-Berthelot, L.-S. Liao, Z.-Q. Jiang, C. Poriol, *Angew. Chem., Int. Ed.* **2019**, *58*, 3848.
- [49] K.-T. Wong, Y.-L. Liao, Y.-T. Lin, H.-C. Su, C.-c. Wu, *Org. Lett.* **2005**, *7*, 5131.
- [50] Q. Wang, F. Lucas, C. Quinton, Y.-K. Qu, J. Rault-Berthelot, O. Jeannin, S.-Y. Yang, F.-C. Kong, S. Kumar, L.-S. Liao, C. Poriol, Z.-Q. Jiang, *Chem. Sci.* **2020**, *11*, 4887.
- [51] Y. Luo, Z. Liu, G. Yang, T. Wang, Z. Bin, J. Lan, D. Wu, J. You, *Angew. Chem., Int. Ed.* **2021**, *60*, 18852.
- [52] C.-c. Wu, T.-L. Liu, W.-Y. Hung, Y.-T. Lin, K.-T. Wong, R.-T. Chen, Y.-M. Chen, Y.-Y. Chien, *J. Am. Chem. Soc.* **2003**, *125*, 3710.
- [53] W. Wei, P. I. Djurovich, M. E. Thompson, *Chem. Mater.* **2010**, *22*, 1724.
- [54] S. C. Moldoveanu, in *Analytical Pyrolysis of Natural Organic Polymers*, 2nd ed., Vol. 20, (Ed: S. C. Moldoveanu), Elsevier, Amsterdam **2021**, p. 3.
- [55] X. Ren, J. Li, R. J. Holmes, P. I. Djurovich, S. R. Forrest, M. E. Thompson, *Chem. Mater.* **2004**, *16*, 4743.
- [56] J.-J. Lin, W.-S. Liao, H.-J. Huang, F.-I. Wu, C.-H. Cheng, *Adv. Funct. Mater.* **2008**, *18*, 485.
- [57] S. Liu, D. Xia, M. Baumgarten, *ChemPlusChem* **2021**, *86*, 36.
- [58] J. Sworakowski, J. Lipiński, K. Janus, *Org. Electron.* **2016**, *33*, 300.
- [59] M. Idris, S. C. Kapper, A. C. Tadler, T. Batagoda, D. S. Muthiah Ravinson, O. Abimbola, P. I. Djurovich, J. Kim, C. Coburn, S. R. Forrest, M. E. Thompson, *Adv. Opt. Mater.* **2021**, *9*, 2001994.
- [60] T. Sajoto, P. I. Djurovich, A. B. Tamayo, J. Oxgaard, W. A. Goddard, M. E. Thompson, *J. Am. Chem. Soc.* **2009**, *131*, 9813.
- [61] X. Zhou, B. J. Powell, *Inorg. Chem.* **2018**, *57*, 8881.
- [62] S. Arroliga-Rocha, D. Escudero, *Inorg. Chem.* **2018**, *57*, 12106.
- [63] C. Tonnelé, M. Stroet, B. Caron, A. J. Clulow, R. C. R. Nagiri, A. K. Malde, P. L. Burn, I. R. Gentle, A. E. Mark, B. J. Powell, *Angew. Chem., Int. Ed.* **2017**, *56*, 8402.
- [64] M. Gao, T. Lee, P. L. Burn, A. E. Mark, A. Pivrikas, P. E. Shaw, *Adv. Funct. Mater.* **2020**, *30*, 1907942.
- [65] R. Coehoorn, P. A. Bobbert, *Phys. Status Solidi A* **2012**, *209*, 2354.
- [66] R. G. Clarkson, M. Gomberg, *J. Am. Chem. Soc.* **1930**, *52*, 2881.
- [67] A. Vlček, S. Zálíž, *Coord. Chem. Rev.* **2007**, *251*, 258.